RSC Advances

PAPER

View Article Online
View Journal | View Issue

Cite this: *RSC Adv.*, 2016, **6**, 107613

Synthesis of europium-doped ZnS nano-crystalline thin films with strong blue photoluminescence†

M. J. Rivera-Medina,[a] J. Hernández-Torres,[b] J. L. Boldú-Olaizola,[c] J. Barreto-Rentería,[c] J. M. Hernández-Alcántara,[c] V. Jancik[d] and J. C. Alonso-Huitrón*[a]

Received 30th September 2016
Accepted 31st October 2016

DOI: 10.1039/c6ra24300b

www.rsc.org/advances

Eu^{2+}-Doped ZnS (ZnS:Eu^{2+}) thin (~550 nm) films with strong and stable blue photoluminescence have been successfully synthesized by a simple and fast ultrasonic spray pyrolysis method. According to X-ray diffraction (XRD) and high resolution scanning electron microscopy (SEM) analysis, the as grown ZnS:Eu^{2+} films are composed of hexagonal wurtzite nanocrystals with average size of ~25 nm, which are preferentially oriented along the (002) direction and agglomerate to form hexagonal facet nanobars with diameters from 50 to 200 nm. These films show a strong blue emission centered at 454 nm, which can be observed with the naked eye under ambient illumination. The intensity of this peak is ~185 times higher than the maximum photoluminescence peak observed from the undoped ZnS films. The presence of the Eu dopant in the valence state Eu^{2+} was confirmed by electron spin resonance (ESR) measurements. The comparison of the high-resolution UV-vis absorption spectra and the PL characteristics of the ZnS:Eu^{2+} films with the pure ZnS films, indicate that the strong blue emission of the ZnS:Eu^{2+} films comes from Eu^{2+} $4f^6 5d \rightarrow 4f^7$ intra-ion transitions.

1. Introduction

Rare earth doped phosphors have been very important for the development of a wide variety of modern luminescent devices such as: fluorescent lamps, solid state lasers, flat panel displays, *etc.* Nowadays, with the combination of rare earth dopants such as Eu^{2+} and Ce^{3+}, it is possible to make activated inorganic phosphors emitting in the blue, green and red colors, for the fabrication of white light emitting diodes (WLEDs) with a good control in the light color balance.[1] Recently the Eu^{2+} ion has been intensively investigated as a blue and blue-green-emitting activator in a wide variety of host materials in the form of powders, nanoparticles or nanocrystals, such as: graphene,[2] $Ba_{1-x}(PO_3)_2$ ($x = 0.005$–0.040),[3] $BaAlBO_3F_2$,[4] Sr_4OCl_6,[5] $Ba_3P_4O_{13}$,[6] zeolite derivative,[7] ZnS,[8] and also in thin films of compounds such as: $12CaO \cdot 7Al_2O_3$,[9] or Ta_2O_5.[10] More recently, due to the high quantum efficiency of the dipole allowed 5d → 4f transitions of divalent europium, it has proven to be an excellent luminescent activator for the development of new KSr_2I_5:Eu crystalline scintillators, with X-ray-excited blue emission.[11]

The luminescent characteristics of Eu^{2+} incorporated in more than 300 different inorganic compounds have been compiled, and it has been shown that the energy of the first $4f^7 \rightarrow 4f^6 5d$ transitions of free Eu^{2+} (4.2 eV or 295 nm) is red shifted by effect of the host crystal,[12] and consequently that the excitation and emission energies can be modulated and improved through changing the composition and structure of the host crystal.[1,12] As a motivation for the present work, it is noteworthy that although in this compilation were included around 35 Eu-doped sulfide compounds, having emission wavelengths in the range from blue (459 nm) to red (680 nm), the Eu-doped ZnS compound was not included in this compilation.[12] This is intriguing since ZnS has been widely used as an excellent host material for a variety of luminescent centers based on transition and rare earth metals such as: Mn, Cu, Co, Ni, Sm,[13–24] and efficient thin film electroluminescent (TFEL) devices have been fabricated with some of these transition metal-rare earth-doped ZnS systems.[14,15] On the other hand, in the literature there are many reports of studies on the structure and photoluminescence (PL) of the ZnS:Eu^{2+} system, in the form of bulk crystals, powders, nanocrystals, nanoparticles and nanowires.[8,25–37] At the beginning the technological efforts were made to obtain stable Eu^{3+} red emission in the ZnS host, however on the basis of electron spin resonance experiments, it was demonstrated that Eu often tends to be stable in the 2+ charge state due to its half filled 4f shell, and that Eu naturally incorporates in single crystals with hexagonal wurtzite lattice of

[a]*Instituto de Investigaciones en Materiales, Universidad Nacional Autónoma de México, A.P.70-360, Coyoacán 04510, Ciudad de México, Mexico. E-mail: alonso@unam.mx*

[b]*Centro de Investigación en Micro y Nanotecnología, Universidad Veracruzana, Boca del Río 94294, Veracruz, Mexico*

[c]*Instituto de Física, Universidad Nacional Autónoma de México, A.P. 20-364, Coyoacán 01000, Ciudad de México, Mexico*

[d]*Centro Conjunto de Investigación en Química Sustentable UAEM-UNAM, Carr. Toluca Atlacomulco km. 14.5, Toluca 50200, Estado de México, Mexico*

† Electronic supplementary information (ESI) available. See DOI: 10.1039/c6ra24300b

ZnS, as Eu^{2+}, substituting Zn^{2+}, without any problem of charge compensation.[25–27] Although it was also found that the limit of solubility of Eu in the ZnS lattice is rather low (does not exceed 0.1%), these works motivated the investigation of the PL characteristics of a wide variety of ZnS:Eu^{2+} nanocrystals, nanoparticles and nanowires. Depending on the method of synthesis, precursors, thermal treatments, size of crystals, crystalline phase (cubic zinc blende or hexagonal wurtzite), *etc.*, these nanostructures may present green,[28–31,37] or blue emission,[8,32–37] or combined blue and green emission.[8,36,37] Most of the methods used for the synthesis of the above mentioned ZnS:Eu^{2+} nanomaterials involve long and complicated processes, and/or thermal treatments. For example, several works use $EuCl_2$, but it is highly sensitive to moisture, and thus hydrothermal or N_2 treatments at 80–120 °C for 15–24 h or sinterization at 800 °C for 3 h are required to obtain the final ZnS:Eu^{2+} nanomaterial.[28–32,34,36] Other methods use Eu_2O_3, which is converted to $Eu(NO_3)_3$ and mixed with $Zn(NO_3)_2$ and thiourea, and then the mixture is kept at 160 °C for 15 h to get the final luminescent product.[34,35] The $Eu(NO_3)_3$ precursor is directly used and mixed with zinc acetate and thioacetamide in a co-precipitation method, but the ZnS:Eu^{2+} phosphors require annealing at 1100 °C to get intense luminescence.[8] $Eu(NO_3)_3$, ZnS and NaCl were used in a simple vapor deposition method, but the furnace where the ZnS:Eu^{2+} nanowires were prepared was heated for different times to 1100 °C in a mixture of Ar and H_2 gases to ensure that all the Eu^{3+} ions were reduced to Eu^{2+}.[37] The $EuCl_3 \cdot 6H_2O$ precursor along with ZnS powder have been used to grow ZnS:Eu^{2+} nanowires by chemical vapor deposition, heating the source materials and the substrate at 800 °C during 10 min under a constant flow of Ar (97%) and H_2 (3%), and then cooling down to room temperature.[33]

On the other hand, in spite of the previously mentioned studies, very little work has been done on ZnS:Eu^{2+} phosphors in the form of thin-film, and the scare works have reported other emission features and not the blue or green emission characteristics of Eu^{2+} ions.[38,39] In one of these works ZnS:Eu,Cl thin films were evaporated by electron gun and incorporated in TFEL devices, with emission bands assigned to transitions within the Eu^{3+} ions.[38] In another work ZnS:Eu,F thin films were prepared by r.f. magnetron sputtering, and incorporated in TFEL devices whose luminous characteristics corresponded also to the emission of Eu^{3+} ions.[39] In the latter case, even for the optimum europium concentration (0.94%) in the sputtering target, for which the highest luminance was obtained, the intensity of the electroluminescence of the ZnS:Eu TFEL devices was much lower than that of the ZnS:Mn devices.[39]

In this work we report a strong blue photoluminescence from ZnS:Eu^{2+} thin films synthesized by a simple, fast and cheap ultrasonic spray pyrolysis method. These films have potential applications for the development of high intensity miniature electroluminescent displays.[14,15]

2. Experimental section

The ZnS:Eu^{2+} films were deposited on glass substrates by the ultrasonic spray pyrolysis technique at atmospheric pressure, using a home-made spray system (see Fig. S1 in the ESI†). To prepare 100 ml of the starting solution, zinc acetate dihydrate $[Zn(CH_3COO)_2 \cdot 2H_2O]$ (0.724 g, 3.30 mmol), 1,3-dimethyl-2-thiourea $[CH_3NHCSNHCH_3]$ (0.521 g, 5.00 mmol) and europium chloride hexahydrate $[EuCl_3\ 6H_2O]$ (0.037 g, 0.10 mmol, 3 molar% of zinc) were mixed as solids. Subsequently, anhydrous methanol (71.2 ml), deionized water (23.8 ml) and acetic acid (5 ml) were added in this exact order. The final concentration of Zn^{2+}, thiourea and Eu^{3+} in this solution is 0.033 M, 0.05 M and 0.001 M, respectively. Based on the thermogravimetric analysis (TGA) of the precursor powders, and the possible reactions carried out from the thermal decomposition of the precursors (see Section 3.1.), the substrate temperature was 450 °C for all the deposits, and air was used as the carrier and director gas with constant flow rates fixed at 1.5 l min^{-1} and 0.3 l min^{-1}, respectively. Under these deposition conditions ~550 nm thick ZnS:Eu^{2+} films were obtained using 10 ml of the precursors solution during 15 min of deposition. All reagents were purchased from Sigma Aldrich and used as received without further purification. The air used for the spray pyrolysis deposition process was provided from an oil free air compressor. Undoped ZnS films were deposited under the same conditions but using a solution without europium chloride.

The TGAs of the precursor powders, were obtained using a TGA Q50000 V3.15 equipment from TA Instruments. The crystalline structure of the films was characterized by X-ray diffraction (XRD). The apparatus used for the XRD measurements was a Bragg–Brentano Rigaku ULTIMA IV diffractometer with an X-ray source of Cu Kα line (0.15406 nm), at a grazing beam configuration (incidence angle of 1°). The surface morphology of the films was investigated by atomic force microscopy (AFM) and scanning electron microscopy (SEM), using a JEOL JSPM-4210 scanning probe microscope and a JEOL 7600F field emission scanning electron microscope (FESEM), respectively. The chemical composition of the films was analyzed by energy dispersive spectroscopy (EDS) using an EDX INCA X-act by OXFORD spectrometer coupled to the SEM equipment. The operating voltage was 10 kV for the FESEM images. EDX major operating parameters were: working current 4.5×10^{-10} A, voltage 10 kV, working distance 6 mm, and the atomic number-absorption–fluorescence method was used for quantitative analysis.

The room temperature photoluminescence characteristics of the films, excitation and emission spectra, were recorded using a Spex Fluoromax spectrofluorometer sensitive in the range from 200 to 850 nm, and provided with a xenon lamp for the excitation light. Some PL spectra were also obtained while exciting the sample with an unfocused beam of 25 mW from a Kimmon He–Cd laser operating at 325 nm (3.81 eV), and collecting the emitted light with an optical fiber connected to the spectrofluorometer. Electron spin resonance (ESR) measurements for the detection of Eu^{2+} in the ZnS:Eu^{2+} films, were made using a JEOL (JES-RE3X) ESR-X-spectrometer, equipped with rectangular cavity and a gas flow cryostat working in the temperature range from 110 to 300 K. The Eu^{2+} ESR spectrum was obtained at 113 K (−160 °C) using a resonance frequency of 9.1 GHz and a magnetic field centered at 330

mT. For the ESR measurements the ZnS:Eu^{2+} films were deposited on KCl single crystalline substrates, in order to avoid the presence of spurious ESR signals due to the paramagnetic impurities (mainly Mn^{2+} and Fe^{2+}) in the glass substrates.

3. Results and discussion

3.1. Film growth

The precursors in the starting solution were zinc acetate dihydrate, 1,3-dimethyl-2-thiourea and europium chloride hexahydrate, which where dissolved in anhydrous methanol (three parts), deionized water (one part) and acetic acid (5%). Based on related studies, the 1,3-dimethyl-2-thiourea was proposed as the source of hydrogen sulfide as it is released gradually by its acidic hydrolysis at elevated temperature and thus it does not cause precipitation of zinc and europium sulfides in the solution.[40] The driving force for the hydrolysis is the difference between the C=S ($\Delta_f H^\circ_{298} = 573$ kJ mol^{-1}) and C=O ($\Delta_f H^\circ_{298} = 789$ kJ mol^{-1}) bond enthalpies.[41] To determine the optimal temperature for the substrate, TGA analyses of the precursors were performed and the obtained TGA curves are shown in Fig. 1. The TGA curve in Fig. 1a is similar to that previously reported,[40] and shows that the 1,3-dimethyl-2-thiourea starts its one-step thermal decomposition, above 100 °C and it decomposes completely at ~235 °C, while Fig. 1b shows that the zinc acetate dihydrate decomposes in two steps. The first mass loss step corresponds to the loss of the two water molecules, and the other step corresponds to the decomposition of the zinc acetate, which decomposes completely at ~250 °C. Although a similar behavior has been reported for the thermal decomposition of this precursor, depending on the rate of heating and gas used, its thermal decomposition may be carried out in three steps and the complete decomposition can be shifted to higher temperatures. For example in helium, the complete decomposition occurs at 300–325 °C.[42] The TGA curve shown in Fig. 1c indicate that europium chloride hexahydrate does not simply decompose, but undergoes first a stepwise dehydration to $EuCl_3 \cdot H_2O$ (25% mass loss), and that rather complex hydrolytic reactions occur resulting in the formation of different mixed chloride hydroxide species until, $EuCl_2OH$ is formed (further 11% mass loss). The final product at 475 °C is the solid EuOCl, which can be recovered from the crucible after thermal analysis. This is in agreement with previously observed results.[43,44]

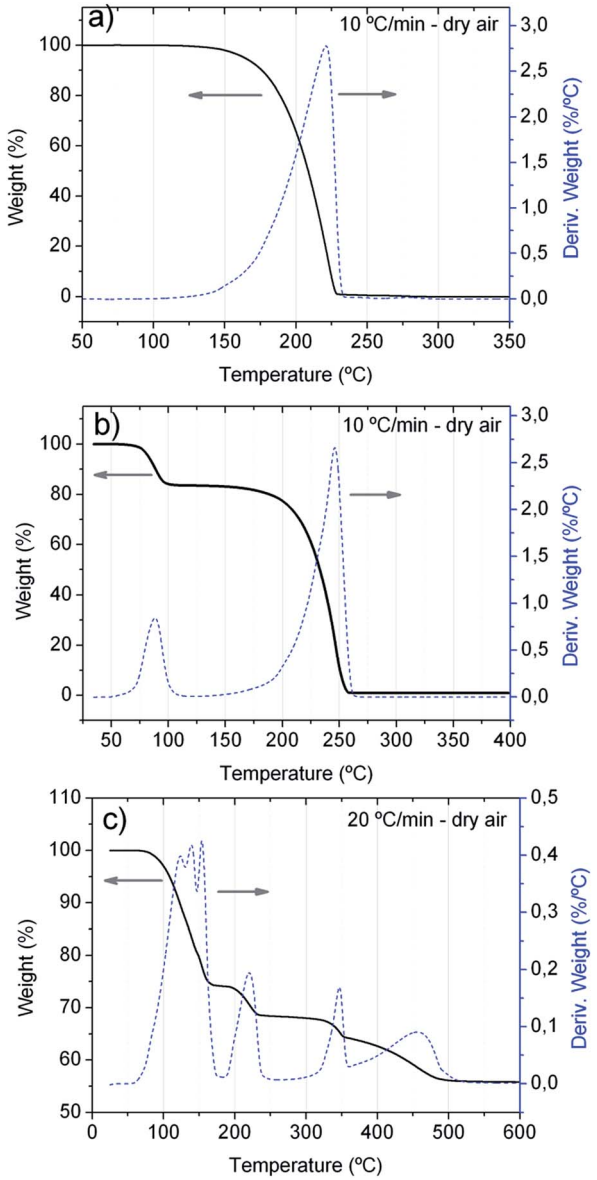

Fig. 1 TG-DTG curves for the (a) 1,3-dimethyl-2-thiourea; (b) zinc acetate dihydrate and (c) europium(III) chloride hexahydrate precursors, evaluated at 10 °C min^{-1} heating rate carried out in a dry air atmosphere.

Based on the TGA characteristics of the precursors and in order to assure the incorporation of Eu in the ZnS films, the substrate temperature of 450 °C was chosen.

When the aerosol droplets of the solution containing all precursors arrive to the heated substrate, several complex hydrolytic and pyrolytic processes and reactions occur that produce many different Zn, S and Eu species and give rise to the film growth. Although we do not have elements to determine the detailed chemical reaction pathways and/or the heterogeneous reactions at the substrate surface that develop the adherent ZnS:Eu^{2+} film, based on related literature we propose the following steps:

$$[CH_3NH]_2C=S + H_2O \xrightarrow{\text{heat}} [CH_3NH]_2C=O + H_2S \quad (1)$$

$$Zn[CH_3CO_2]_2 \cdot 2H_2O + H_2S \xrightarrow{\text{heat}} ZnS + 2[CH_3COOH] + 2H_2O \quad (2)$$

$$EuCl_3 \cdot 6\,H_2O \xrightarrow{\text{heat}} EuOCl + 2HCl + 5H_2O \quad (3)$$

$$6EuOCl + 7H_2S \xrightarrow{\text{heat}} 6\,EuS + 6HCl + 4H_2O + SO_2 \quad (4)$$

In the first step, the hydrolysis of the 1,3-dimethyl-2-thiourea produces H_2S which reacts with $Zn[CH_3CO_2]_2$ and EuOCl forming the resulting ZnS:Eu^{2+} film. The europium atoms are incorporated in the ZnS framework as a substitutional impurity. However the most interesting thing about this synthesis is the

fact that although we start from europium in the oxidation state (III) and the preparation of the films is made at high temperature and in the presence of air, the europium gets reduced to Eu^{2+}, which is highly counterintuitive. The mechanism of this reduction is however, unclear. It was recently demonstrated, that from the aqueous solution of praseodymium(III) iodide and thiourea crystallizes $PrI_3 \cdot 9H_2O \cdot 0.5$ thiourea. Furthermore, the thiourea has no interaction with the metal ion, but rather forms hydrogen bonds with the coordinated water molecules.[45] In acidic aqueous solution of $EuCl_3$, the europium ions form a similar hydrated cation $-Eu(H_2O)_6^{3+}$ and thus direct interaction of the Eu^{3+} ions with thiourea in the starting solution can be discarded. On the other hand, reduction of Eu_2O_3 to EuS under H_2S atmosphere can be achieved, however at 1150 °C. In this reaction H_2S acts also as the reducing agent and elemental sulfur is formed, but if this reaction is performed at 600 °C, Eu_2S_3 and water are the only products.[46] However, thermal process involving H_2S generated from thiourea has been recently used in the reduction of aromatic nitro- to amino-compounds.[47] Thus we propose that in this case the Eu^{3+} is probably in the form of EuOCl and is reduced by H_2S to Eu^{2+} and EuS is formed. Due to the reaction conditions, during the reduction, H_2S is probably oxidized directly to SO_2. To the best of our knowledge, this is the first example of a direct thermal reduction of Eu^{3+} to Eu^{2+} during the synthesis of ZnS under aerobic conditions.

3.2. Structure, morphology and chemical composition

Fig. 2 shows the XRD patterns for the ZnS:Eu^{2+} film, and that of an un-doped ZnS film. The XRD patterns indicate that both, the Eu-doped and un-doped films are polycrystalline with a preferential orientation at $2\theta = 28.54°$, and a secondary diffraction peak at $2\theta = 51.8°$, which correspond to the (002) and (103) planes, respectively, of the hexagonal wurtzite ZnS crystalline structure (card number 00-005-0492 from PDF-2-(2004) data base). All the other smaller XRD peaks also correspond to the hexagonal phase of ZnS.

The average crystallite size (D) of each film was assessed using the Debye–Scherrer formula, and the lattice parameters for the hexagonal structure (a and c), and these parameters were: $D = 24.0$ nm, $a = 3.862$ Å, $c = 6.225$ Å and $D = 24.8$ nm, $a = 3.830$ Å, $c = 6.240$ Å, for the ZnS:Eu^{2+} and ZnS films, respectively. The structure of the ZnS:Eu^{2+} film is consistent with the results found in some of the earliest investigations which demonstrated that Eu enters in the hexagonal wurtzite lattice of ZnS bulk crystals, as Eu^{2+}, substituting Zn^{2+}.[26]

The variations in the lattice parameters are expected since the ionic radius of Eu^{2+} (1.14, 1.17 Å)[48,49] is larger than that of Zn^{2+} ion (0.74 Å), and when the Eu^{2+} ions replace the Zn^{2+} ions, a lattice distortion in the structure is produced.[35] However the small variations in these parameters indicate that the amount of Eu^{2+} ions incorporated in the ZnS matrix is very small.

Fig. 3 depicts the FESEM micrographs for the ZnS and ZnS:Eu^{2+} films. The image in Fig. 3a appears darker because the probe current was lower than in the others (Fig. 3b–d). The micrographs in Fig. 3b–d were obtained at higher probe current

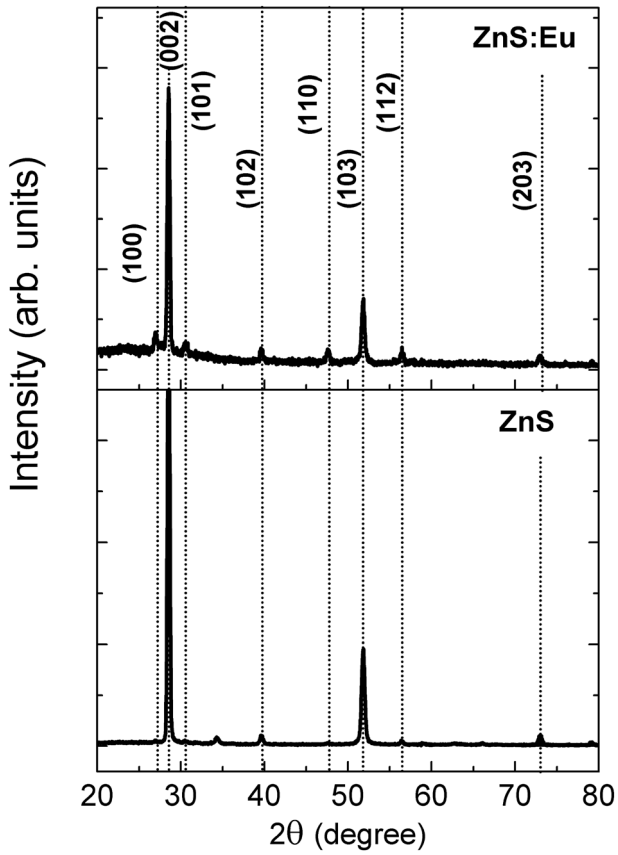

Fig. 2 Typical X-ray diffraction patterns for the ZnS and ZnS:Eu^{2+} films, as deposited by ultrasonic spray pyrolysis, at substrate temperature of 450 °C.

in order to get deeper topographic information. The micrographs in Fig. 3a and b are planar surface and inclined cross section views, respectively, for the un-doped ZnS film. As these micrographs show this film consist of well packed hexagonal shaped bars with diameters in the range from 100 to 300 nm, which grew mainly oriented in the z-axis perpendicular to the substrate. The micrographs in Fig. 3c and d, correspond to the ZnS:Eu^{2+} film, and show that the Eu^{2+} doped films had a similar growth, although in this case the diameters of the hexagonal shaped bars are smaller, in the range from 50 to 200 nm, approximately. The regular and highly oriented hexagonal structures observed in the FESEM images of the films are in good agreement with the hexagonal wurtzite phase and preferential orientation observed in the XRD spectra. This consistency indicates that during the growth of the films, the crystalline grains aggregate to form the hexagonal bars. The same morphology of agglomerates of small grains was observed from the AFM analysis of the ZnS:Eu^{2+} films (see the AFM images with different zooms in Fig. S2 in the ESI†). The size of the grains was evaluated in different zones of the AFM images (see Fig. S3 in the ESI†), and the average size was ~26.5 nm, which is very close to the average size of the crystallites calculated from the XRD analysis.

An attempt was made to detect the Eu atoms incorporated the ZnS:Eu^{2+} films, by techniques such as X-ray photoelectron

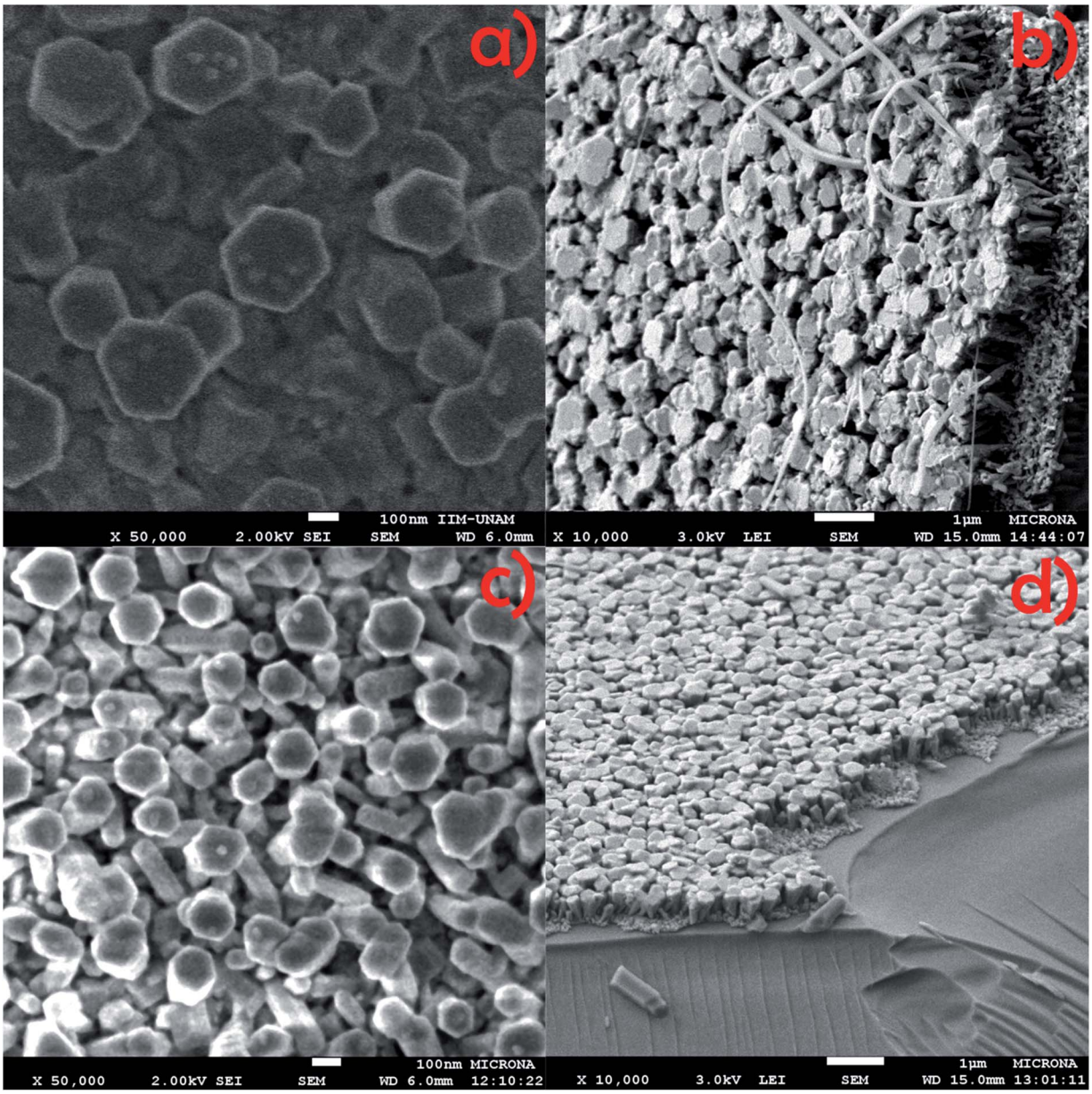

Fig. 3 SEM micrographs for the ZnS and ZnS:Eu^{2+} films deposited by USP: ZnS film (a) planar view and (b) cross view with a rotation of 188.4° and 6.1° of inclination. ZnS:Eu^{2+} film (c) planar view and (d) cross view with a rotation of 94.6° and 8.0° of inclination.

spectroscopy, and energy dispersive spectroscopy. However the absence of any signal related to Eu in the spectra obtained for the analyzed films, indicated that the amount of Eu incorporated in the ZnS matrix of the films was below the limit of detection (~1 at%) of the equipment utilized for these analyses. The low concentration of Eu in our ZnS:Eu^{2+} films is also consistent with the low limit of solubility reported for Eu in ZnS single crystals.[26] In order to confirm the existence of trace amounts of Eu^{2+} in the ZnS:Eu^{2+} films, ESR measurements were carried out.

Fig. 4 shows the ESR spectrum of the ZnS:Eu^{2+} film. The observed spectrum is similar to that reported in previous works for Eu^{2+} substituting Zn^{2+} sites in the hexagonal wurtzite-phase ZnS lattice,[26,33] with the principal line at 325.2 mT and a *g*-value of 2.0041. As it is known, any ESR signal associated with europium is originated from Eu^{2+} ions in the $4f^7$ [$^7S_{7/2}$] ground state configuration.[50]

3.3. Optical properties

3.3.1 Optical absorption. Fig. 5 shows the optical absorption spectra of the Eu^{2+} doped ZnS and un-doped films. The subtraction of the two spectra is also shown in the inset of this figure. For the un-doped ZnS film, there is a sharp absorption peak at 333 nm (3.73 eV). Since bulk ZnS crystal has a direct band gap of 3.68–3.77 eV,[51–54] this absorption peak can be identified as due to interband or band edge absorption in which the 3.73 eV photons excite electrons from the valence band to

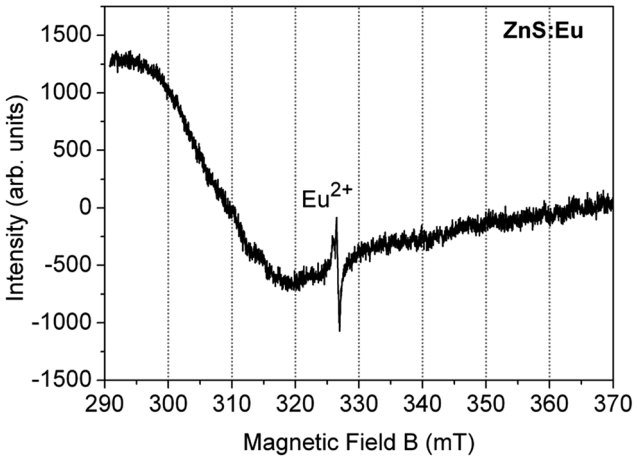

Fig. 4 Electron spin resonance (ESR) spectrum of the ZnS:Eu^{2+} film obtained at 113 K (−160 °C) using a resonance frequency of 9.1 GHz and a magnetic field centered at 330 mT. The ESR line of Eu^{2+} is observed at 325.2 mT.

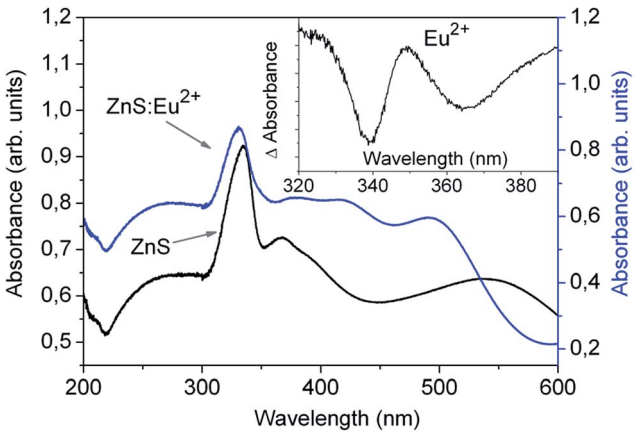

Fig. 5 UV-vis absorbance spectra of ZnS and ZnS:Eu^{2+} films. The inset shows the subtraction of the ZnS:Eu^{2+} and the ZnS spectra.

the conduction band of the ZnS film. The smaller absorption peak located at 367.6 nm (3.37 eV) in the spectrum of the ZnS film can be due to absorption of photons that excite electrons from the valence band to localized donor states below the conduction band due to vacancies of sulfur and/or interstitials of zinc.[55,56] For the Eu doped ZnS thin film there is a sharp absorption peak at 331 nm (3.75 eV) which can be also assigned to interband absorption of the ZnS matrix. However in this case there is also an absorption shoulder located around 350 nm (3.54 eV), which is the position of the peak resulted from the subtraction of the two spectra shown in the inset of Fig. 5. Since this absorption feature is absent in the absorption spectrum of the un-doped ZnS film, we can assume that this is due to the Eu^{2+} ions incorporated in the ZnS matrix. As it has been shown in some recent works, when Eu^{2+} ions are incorporated in some compounds, they are stable on the divalent site and the energy of the lowest Eu^{2+} $4f^6$5d level is always below the bottom of the conduction band of the compound.[12,57] Thus, since our XRD

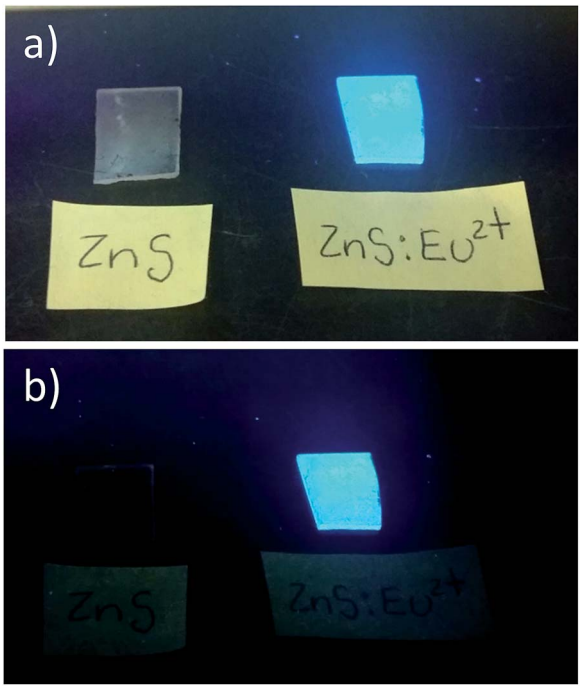

Fig. 6 Photographs of ZnS and ZnS:Eu^{2+} thin films deposited on glass, excited with a UV lamp at 254 nm, in (a) bright room and (b) in a dark room. The sample with the ZnS:Eu^{2+} film shows an intense blue photoluminescence.

and ESR results indicate that the Eu^{2+} ions in the ZnS film are occupying the divalent Zn^{2+} sites, we can infer that the absorption shoulder is due to the absorption of photons that generate transitions of electrons from the valence band of the ZnS matrix to the Eu^{2+} $4f^6$5d levels, which in this case are ~0.21 eV below the bottom of the conduction band of the ZnS compound.

3.3.2 Photoluminescence. Fig. 6a and b show the eye-visible photoluminescence (PL), in a bright and dark room, respectively, of the ZnS and ZnS:Eu^{2+} films deposited on glass substrates, which were excited under UV irradiation with a 254 nm lamp. As can be seen the ZnS:Eu^{2+} shows a strong blue PL, meanwhile the ZnS film in the bright room instead of showing any blue PL, only reflects and/or scatters some white light.

The PL spectra of both films, collected with an optical fiber under excitation with the 325 nm beam of the He-Cd laser are shown in Fig. 7. From this figure and the inset, it is clearly seen that the PL of the ZnS:Eu^{2+} film is much higher than that of the ZnS film, and the main peaks are located at 454 and 527 nm, respectively. The ratio of the intensity of the main PL peaks is around 185. The green emission band of the un-doped ZnS film, centered at 527 nm can be assigned to the radiative electron transfer from sulfur vacancies to interstitial sulfur states.[8,56] The strong blue PL from the ZnS:Eu^{2+} films, consists of a broad emission centered at 454 nm, with a full-width at half-maximum intensity of (FWHM) of approximately 94 nm.

Fig. 8 shows the PL emission spectra obtained for different excitation wavelengths. As can be seen from this figure the PL

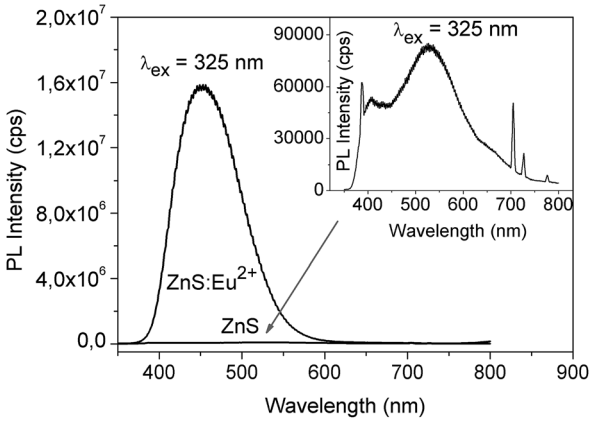

Fig. 7 Room temperature PL spectra the ZnS and ZnS:Eu^{2+} films excited at 325 nm with a He-Cd laser. The inset exhibits a zoom of the PL spectrum of the ZnS film.

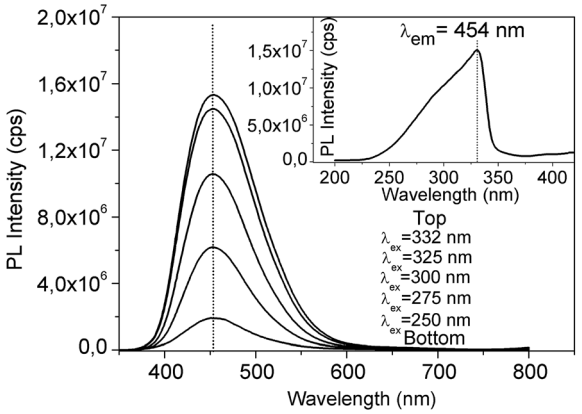

Fig. 8 Room temperature emission spectra of the ZnS:Eu^{2+} film for different excitation wavelengths coming from the xenon lamp of the Spex spectrofluorometer. The inset shows the excitation spectrum for the emission peak at 454 nm.

intensity increases as the excitation wavelength increases from 250 to 332 nm, and the position of the PL peak is maintained around 454 nm (2.73 eV). The excitation spectrum of the main PL peak at 454 nm is also shown in the inset of Fig. 8. The excitation spectrum indicates that the maximum intensity of the 454 nm peak is obtained for the excitation wavelength of λ_{exc} = 331 nm. Since this excitation wavelength corresponds to photons with energy equal to 3.75 eV, and this energy correspond to the band gap of the ZnS:Eu^{2+} films we can assume that the PL is efficiently excited when the excitation energy is absorbed by the host lattice ZnS, and then it is transferred to the Eu^{2+} activator, as generally occurs in semiconductor phosphors with luminescent centers.[58]

According to the compilation made by P. Dorenbos on the emission spectra of Eu^{2+} in inorganic compounds, there are three types of Eu^{2+} related emissions, which are, (1) normal broad band dipole and spin allowed d–f emission, (2) ff narrow and (3) "anomalous" Eu^{2+} emission.[12] The most common type of emission observed in the majority of the compounds is the normal broad d–f emission, in which the radiative transition starts from the $4f^6$ [$^7F_0$] 5d excited state and ends in the $4f^7$ [$^8S_{7/2}$] ground state of Eu^{2+}.[12] The peak wavelength (λ_{em}) and the full width at half maximum intensity (FWHM) at room temperature of this type of emission depend on the composition, crystalline structure and morphology of the host, because the shift and splitting of the outermost 5d levels of the Eu^{2+} ions are very sensitive to the local crystal field, and the phonon energies also depend on the crystal lattice.[7,12,59] For example, for Eu^{2+} ions incorporated in microporous zeolite derivatives, the PL spectra have λ_{em} = 450 nm and FWHMs in the range from 85 nm to 150 nm, depending on the synthesis conditions.[7] For $12CaO \cdot 7Al_2O_3$ thin films doped with Eu^{2+} ions λ_{em} = 444 nm and FWHM ≈ 60 nm.[9] For Eu^{2+} ions in $BaAlBO_3F_2$, λ_{em} ≈ 450 nm and the blue luminescence is very narrow FWHM ≈ 38 nm.[4]

Based on all these previous and related works, the strong and broad blue PL centered at 454 nm emitted from our ZnS:Eu^{2+} films, can be ascribed to intra-ion electronic transitions of Eu^{2+} from the $4f^65d$ excited state to the $4f^7$ ground state.

Given the absorption and PL excitation and emission characteristics of our ZnS:Eu^{2+} films, we can propose the following excitation–emission mechanisms. (1) First the incoming radiation with energy equal or higher than 3.75 eV (λ_{exc} = 331 nm), excite electrons from the valence band to the conduction band of the ZnS host, and also from the $4f^7$ ground state of Eu^{2+} to the conduction band of ZnS.[8] (2) Then the photogenerated electrons lose energy and decay to the $4f^65d$ levels of the luminescent Eu^{2+} ions. (3) Finally the electrons suffer radiative transitions to the $4f^7$ Eu^{2+} levels. In order to have more evidence of the energy transfer from the ZnS host to the $4f^65d$ levels of the Eu^{2+} ions, it is necessary to make further studies such as lifetime analysis of the PL.

4. Conclusions

ZnS:Eu^{2+} thin films that display intense blue PL at room temperature have been successfully synthesized by a simple and fast ultrasonic spray pyrolysis method. The as deposited ZnS:Eu^{2+} films are composed of hexagonal wurtzite nanocrystals with an average size of ~25 nm, which agglomerate to form hexagonal facet nanobars. The incorporation of the Eu dopant atoms in the valence state Eu^{2+} was confirmed by ESR measurements. These measurements along with the absorption and PL characteristics of the films indicate that the efficient blue luminescent comes from intra-ion transitions of Eu^{2+} ions incorporated in the wurtzite ZnS matrix. The high intensity and the emitting color of these ZnS:Eu^{2+} films deposited by this relatively simple and cheap technique ensures their potential application as ideal candidates for modern flat panel electroluminescent displays.

Acknowledgements

The authors want to acknowledge the technical assistance of M. Sc. A. Tejeda, D. Cabrero, C. Flores, Dr O. Novelo, M. Sc. J. Romero-Ibarra, J. M. García-León and Fernando Silvar of IIM-

UNAM, M. Sc. V. Gómez-Vidales of I. Q.-UNAM, and M. Sc. Angelica Gutierrez Franco of MICRONA-UV. This research work was partially supported under project PAPIIT-UNAM number IG100614-2.

References

1 G. Li, Y. Tian, Y. Zhao and J. Lin, *Chem. Soc. Rev.*, 2015, **44**, 8688–8713.
2 B. Park, S. J. Kim, J. Lim, S. Some, J. Park, S. Kim, C. Kim, T. J. Lee and S. C. Jun, *J. Mater. Chem. C*, 2015, **3**, 4030–4038.
3 Z.-C. Wu, H.-H. Fu, J. Liu, S.-P. Kuang, M.-M. Wu, J.-G. Xu and X.-J. Kuang, *RSC Adv.*, 2015, **5**, 42714–42720.
4 Z. Tao, Y. Huang, P. Cai, S. Il Kim and H. J. Seo, *Opt. Mater.*, 2014, **37**, 287–292.
5 S. Gwak, P. Arunkumar and W. Im, *J. Phys. Chem. C*, 2014, **118**, 2686–2692.
6 X. Zhang, F. Meng, W. Li and H. J. Seo, *Ceram. Int.*, 2013, **39**, 8975–8978.
7 X. Yang, T. S. Tiam, X. Yu, H. V. Demir and X. W. Sun, *ACS Appl. Mater. Interfaces*, 2011, **3**, 4431–4436.
8 X. Zhang and L. Wang, *Chalcogenide Lett.*, 2015, **12**, 435–440.
9 H. Zhu, Y. Liu, D. Yan, H. Bian, S. Li, C. Liu, C. Xu and X. Wang, *Opt. Mater.*, 2014, **36**, 1771–1775.
10 K. Miura, Y. Arai and O. Hanaizumi, *Mater. Sci. Appl.*, 2015, **6**, 676–680.
11 L. Stand, M. Zhuravleva, G. Camarda, A. Lindsey, J. Johnson, C. Hobbs and C. L. Melcher, *J. Cryst. Growth*, 2016, **439**, 93–98.
12 P. Dorenbos, *J. Lumin.*, 2003, **104**, 239–260.
13 B. Bodo, D. Prakash and P. K. Kalita, *Int. J. Appl. Phys. Math.*, 2012, **2**, 181–183.
14 E. B. Ramírez, M. Bizarro and J. C. Alonso, *Thin Solid Films*, 2013, **548**, 255–258.
15 G. Boutaud, W. M. Cranton, D. C. Koutsogeorgis, R. M. Ranson, C. Tsakonas and C. B. Thomas, *Mater. Sci. Eng., B*, 2009, **165**, 202–206.
16 P. Thiyagarajan, M. Kottaisamy, K. Sethupathi and M. S. R. Rao, *Displays*, 2009, **4**, 1–5.
17 C. Falcony, M. Garcia, A. Ortiz and J. C. Alonso, *J. Appl. Phys.*, 1992, **72**, 1525–1528.
18 X. Lu, C. Chen, S. Husurianto and M. D. Koretsky, *J. Appl. Phys.*, 1999, **85**, 4154–4159.
19 M. Kuppayee, G. K. V. Nachiyar and V. Ramasamy, *Mater. Sci. Semicond. Process.*, 2012, **15**, 136–144.
20 R. Sarkar, C. S. Tiwary, P. Kumbhakar and A. K. Mitra, *Phys. B*, 2009, **404**, 3855–3858.
21 H. Hu and W. Zhang, *Opt. Mater.*, 2006, **28**, 536–550.
22 W. Chen, J. Z. Zhang and A. G. Joly, *J. Nanosci. Nanotechnol.*, 2004, **4**, 919–947.
23 P. Yang, M. Lu, D. Xu, D. Yuan, C. Song, S. Liu and X. Cheng, *Opt. Mater.*, 2003, **24**, 497–502.
24 P. Yang, M. Lu, D. Xu, D. Yuan and G. Zhou, *J. Lumin.*, 2001, **93**, 101–105.
25 M. Godlewski and D. Hommel, *Phys. Status Solidi*, 1986, **95**, 261–268.
26 K. Swiatek, M. Godlewski, D. Hommel and H. Hartmann, *Phys. Status Solidi*, 1989, **114**, 127–133.
27 K. Swiatek, M. Godlewski and D. Hommel, *Phys. Rev. B: Condens. Matter Mater. Phys.*, 1990, **42**, 3628–3633.
28 S. J. Xu, S. J. Chua, B. Liu, L. M. Gan, C. H. Chew and G. Q. Xu, *Appl. Phys. Lett.*, 1998, **73**, 478–480.
29 S. Liu, H. Q. Guo, Z. H. Zhang, F. Q. Liu and Z. G. Wang, *Chin. Phys. Lett.*, 2000, **17**, 609–611.
30 W. Chen, J.-O. Malm, V. Zwiller, Y. Huang, S. Liu, R. Wallenberg, J.-O. Bovin and L. Samuelson, *Phys. Rev. B: Condens. Matter Mater. Phys.*, 2000, **61**, 11021–11024.
31 W. Chen, J.-O. Malm, V. Zwiller, R. Wallenberg and J.-O. Bovin, *J. Appl. Phys.*, 2001, **89**, 2671.
32 G. Sharma, S. Do Han, S. P. Khatkar, V. B. Taxak and Y. W. Rhee, *ECS Trans.*, 2006, **1**, 7–12.
33 S. Y. Lee, Y. H. Shin, Y. Kim, S. Kim and S. Ju, *J. Lumin.*, 2011, **131**, 1336–1339.
34 K. Ashwini, C. Pandurangappa and B. M. Nagabhushana, *Phys. Scr.*, 2012, **85**, 65706.
35 K. Ashwini, Yashaswini and C. Pandurangappa, *Opt. Mater.*, 2014, **37**, 537–542.
36 L. Ma, K. Jiang, X. T. Liu and W. Chen, *J. Appl. Phys.*, 2014, **115**, 103104.
37 B. Cheng and Z. Wang, *Adv. Funct. Mater.*, 2005, **15**, 1883–1890.
38 M. K. Jayaraj and C. P. G. Vallabhan, *J. Electrochem. Soc.*, 1991, **138**, 1512–1516.
39 M. Aozasa, H. Chen and A. Keiichi, *Thin Solid Films*, 1991, **199**, 129–138.
40 L. Abate, A. Chisari, R. Maggiore and G. Siracusa, *Thermochim. Acta*, 1988, **136**, 153–161.
41 J. E. Huheey, E. A. Keiter and R. L. Keiter, *Inorganic Chemistry: Principles of Structure and Reactivity*, Pearson, 1997.
42 T. Arii and A. Kishi, *Thermochim. Acta*, 2003, **400**, 175–185.
43 P. A. Lawson and N. A. Stump, *Spectrosc. Lett.*, 2011, **44**, 412–417.
44 S. J. Lyle and W. A. Westall, *Thermochim. Acta*, 1983, **68**, 51–58.
45 T. A. Antonenko, L. Y. Alikberova and D. V. Albov, *Acta Crystallogr., Sect. E: Struct. Rep. Online*, 2012, **68**, m110.
46 R. D. Archer and W. N. Mitchel, in *Inorganic Syntheses*, ed. E. I. Muetterties, McGraw-Hill International, 1967, pp. 77–79.
47 M. Lv, G. Lu and C. Cai, *Asian J. Org. Chem.*, 2015, **4**, 141–144.
48 Y. Q. Jia, *J. Solid State Chem.*, 1991, **187**, 184–187.
49 R. D. Shannon, *Acta Crystallogr., Sect. A: Cryst. Phys., Diffr., Theor. Gen. Crystallogr.*, 1976, **32**, 751–767.
50 M. P. Thi, N. Ruelle, E. Tronc, D. Simons and D. Vivien, *Jpn. J. Appl. Phys.*, 1994, **33**, 1876–1884.
51 H. C. Ong and R. P. H. Chang, *Appl. Phys. Lett.*, 2001, **79**, 3612–3614.
52 T. Yamamoto, S. Kishimoto and S. Iida, *Phys. B*, 2001, **308–310**, 916–919.
53 G. S. Harish and P. Sreedhara Reddy, *Phys. B*, 2015, **473**, 48–53.

54 B. Bodo, D. Prakash, P. K. Kalita and A. X. R. D. Study, *Int. J. Appl. Phys. Math.*, 2012, **2**, 181–183.
55 D. Denzler, M. Olschewski and K. Sattler, *J. Appl. Phys.*, 1998, **84**, 2841.
56 X. Wang, J. Shi, Z. Feng, M. Li and C. Li, *Phys. Chem. Chem. Phys.*, 2011, **13**, 4715–4723.
57 P. Dorenbos, *J. Lumin.*, 2008, **128**, 578–582.
58 G. Blasse, *J. Alloys Compd.*, 1995, **225**, 529–533.
59 X. Piao, K. I. Machida, T. Horikawa and B. Yun, *J. Lumin.*, 2010, **130**, 8–12.